Tensile strength of zinc oxide films measured by a microbridge method

C.W. Ong,[a] D.G. Zong, M. Aravind, and C.L. Choy
Department of Applied Physics and Materials Research Centre, The Hong Kong Polytechnic University, Hung Hom, Kowloon, Hong Kong, People's Republic of China

D.R. Lu
State Key Laboratory of Transducer Technology, Shanghai Institute of Metallurgy, Academy of Sciences, Shanghai, People's Republic of China

(Received 28 May 2003; accepted 16 July 2003)

Double-layered ZnO/silicon nitride microbridges were fabricated for microbridge tests. In a test, a load was applied to the center of the microbridge specimen by using a microwedge tip, where the displacement was recorded as a function of load until the specimen broke. The silicon nitride layer in the structure served to enhance the robustness of the specimen. By fitting the data to a theory, the elastic modulus, residual stress, and tensile strength of the ZnO film were found to be 137 ± 18 GPa, –0.041 ± 0.02 GPa, and 0.412 ± 0.05 GPa, respectively. The analysis required the elastic modulus, internal stress, and tensile strength of the silicon nitride layer. They were measured separately by microbridge tests on single-layered silicon nitride microbridges. The measured tensile strength of the ZnO films represents the maximum tolerable tensile stress that the films can sustain when they are used as the functional component in devices.

I. INTRODUCTION

There is a recent intention to use zinc oxide (ZnO) films to serve as the piezoelectric actuating or sensing elements in microelectromechanical systems, transducers, surface acoustic wave filters, and thin film bulk acoustic wave resonators.[1–3] A ZnO film is inherently brittle and has the risk of fracture when it is used in a micro-sized device. Therefore, the knowledge of the fracture properties of thin piezoelectric ceramic films is important when using them in the above-mentioned devices.[4] To date, most of the experiments for examining the fracture properties of ceramics are designed for bulk samples,[5,6] but investigations on film samples are seldom reported. This is due to the difficulty of extracting the mechanical properties of a thin film from the data of a measurement with the presence of the substrate. Although in principle, measurements can be made directly on a free-standing film sample obtained by removing the substrate material (e.g., substrate-free tensile tests and bulge tests),[7,8] nevertheless, the tests are highly tedious because of the fragility of the substrate-free specimens.

In this paper, we present the results of the measurements of the elastic modulus, internal stress, and tensile strength of magnetron-sputtered ZnO films by using a microbridge method.[9,10] The tensile strength of the ZnO films is most concerned because it represents a limitation of the maximum stress that can be sustained by a film used in a device. In a microbridge test, a sample was made in the form of a double-layered ZnO/silicon nitride microbridge. The silicon nitride layer was introduced to enhance the robustness of the specimen. During the test, a load was applied to the center of the microbridge until it fractured. By fitting the load-displacement data to a theory, the above-mentioned mechanical properties of the ZnO films were determined. In the analysis for a double-layered microbridge, the elastic modulus, internal stress, and tensile strength of the silicon nitride film must be known and were measured separately by another set of microbridge tests on single-layered silicon nitride microbridges. The elastic modulus of the ZnO and silicon nitride films was also measured by conventional nanoindentation methods to compare with the results obtained by using the microbridge tests. The results were discussed and compared with other relevant data published in the literature.

II. EXPERIMENTAL

Silicon nitride films were deposited on *p*-type (100) Si wafers by low-pressure chemical vapor deposition (LPCVD) in an ambient of $SiCl_2H_2$ and NH_3 gases (6:1)

[a]Address all correspondence to this author.
e-mail: apacwong@inet.polyu.edu.hk

at 840 °C and 170 mtorr. The silicon nitride films were postannealed at 1100 °C in nitrogen gas for 2 h. A photolithography/dry etching process was carried out to open windows on one side. The exposed silicon substrate material was etched by KOH at 80 °C such that silicon nitride membranes were formed. Photolithography/dry etching process was carried out to produce arrays of silicon nitride microbridges (length l from 86 to 89 μm, width b from 14 to 21 μm, and thickness $h_{SiN} = 0.40$ μm).

ZnO film was deposited onto the silicon nitride microbridges by magnetron sputtering, such that double-layered ZnO/silicon nitride microbridges were produced. A 2-inch zinc disc was used as the target. The radio-frequency (rf) power, ambient pressure of oxygen and argon gases (7:3), and substrate temperature were set at 80 W, 7 mtorr, and 400 °C, respectively. The deposition time was 3 h. The dimensions of the double-layered microbridges were 35–40 μm in length and 14–21 μm in width. The thickness of the ZnO layer (h_{ZnO}) was 0.64 μm, as determined by scanning electron microscopy (SEM).

A Nano Indenter IIs system (Nano Instrument Inc., TN) equipped with a diamond wedge tip (edge width = 30 μm) was used for the microbridge tests. The wedge edge is wider than the microbridges samples and is aligned along the width of the specimen, allowing one-dimensional modeling of the process. The tip proceeded with a speed of 50 or 20 nm s^{-1}, corresponding to single-layered silicon nitride or double-layered ZnO/silicon nitride, respectively. The displacement was recorded accordingly until the specimen broke. Conventional nanoindentation tests were also conducted at the point with the coexistence of the substrate. The tests were performed with the use of a three-sided Berkovich diamond tip. The elastic modulus values thus attained were compared with the results of the microbridge tests. According to the model of Oliver *et al.*,[11] the nanoindentation elastic modulus is

$$E_{\text{indent}} = \frac{2(1-\nu^2)}{S}\sqrt{\frac{A(h_c)}{\pi}} \quad , \tag{}$$

where S is slope of the unloading curve evaluated at the maximum contact depth h_c, and $A(h_c)$ is the contact area at the maximum load. The Poisson's ratio of the film ν is assumed to be 0.25.

III. THEORY

A. Single-layered silicon nitride microbridges

The mechanical properties of the silicon nitride film must be known for extracting the mechanical properties of the ZnO film by analyzing the load–displacement data of a ZnO/silicon nitride bilayer. We therefore summarize in this section the theoretical formulation for a single-layered microbridge test according to Ref. 10.

The x axis is set to align along the central line of a microbridge as shown in Fig. 1(a). The thickness, length, and width of the microbridge are represented by h_{SiN}, l, and b, respectively. For a vertical load per unit width (Q) applied to the midpoint of the microbridge at $x = l/2$, the vertical displacement (z) is:

$$w(l/2) = -\frac{Q\tanh(kl/2)}{2N_x k} + \frac{Ql}{4N_x} - \frac{M_o}{N_x}\left[\frac{1}{\cosh(kl/2)} - 1\right] + S_{PN}(N_x - N^r{}_{SiN}) + S_{PP}\frac{Q}{2} - S_{PM}M_o \quad . \tag{1}$$

In this equation, $k \equiv \sqrt{(12N_x)/(E_{SiN}h_{SiN}{}^3)}$, where E_{SiN} is the elastic modulus of silicon nitride, N_x the total force per unit width acting along the x direction, $N^r{}_{SiN}$ the residual force per unit width, and M_o the bending moment per unit width acting on the cross section at $x = 0$ [Fig. 1 (b)]. Two additional simultaneous equations correlating M_o and N_x can be derived and expressed as:

$$M_o = \frac{S_{MN}N_x(N_x - N^r{}_{SiN}) + \frac{S_{MP}QN_x}{2} + \frac{Q}{2}\left[\frac{1}{\cosh(kl/2)} - 1\right]}{S_{MN}N_x + k\tanh(kl/2)} \quad , \tag{2}$$

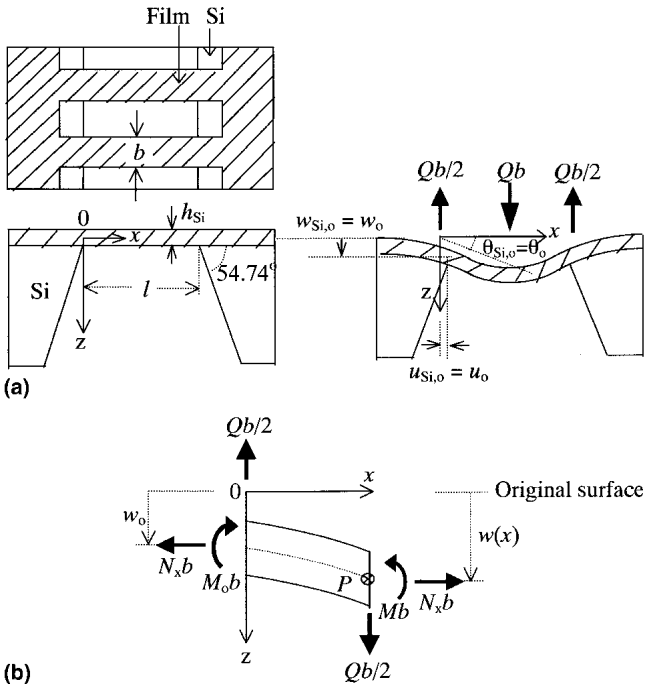

FIG. 1. (a) Schematic presentation of the configuration of a single-layered silicon nitride microbridge and the coordination system. (b) Moments and forces acting on a segment.

$$S_{NN}(N_x - N^r_{SiN}) + S_{NP}\frac{Q}{2} - S_{NM}M_o = \Theta - \frac{l(N_x - N^r_{SiN})}{2E_{SiN}h_{SiN}} \quad . \tag{3}$$

In Eq. (3), Θ is defined to be

$$\Theta = \frac{1}{8k}[(\chi^2 + \xi^2 + 2\zeta^2)kl + 8(\chi - \xi)\zeta \sinh(kl/2) + 2\chi\,\xi\,kl\cosh(kl) + (\chi^2 + 2\chi\xi - \xi^2 + 8\xi\zeta)\sinh(kl) + \xi^2\sinh(2kl)] \quad , \tag{4}$$

where

$$\chi = -\frac{Q\sinh(kl/2) + M_o k}{N_x \sinh(kl)} \quad , \tag{5}$$

$$\xi = \frac{M_o k}{N_x \sinh(kl)} \quad , \tag{6}$$

$$\zeta = \frac{Q}{2N_x} \quad . \tag{7}$$

S_{ij} (i, j = N, P, and M) in Eqs. (1)–(3) are the compliances of silicon. The terms containing S_{ij} take account for the deformability of the silicon substrate. According to the results of finite element analysis:[10]

$$S_{NN} = 0.0545\ \mu m^2\ mN^{-1} \quad ,$$
$$S_{PP} = 0.1373\ \mu m^2\ mN^{-1} \quad ,$$
$$S_{MM} = 0.4173\ mN^{-1} \quad ,$$
$$S_{NP} = S_{PN} = 0.0537\ \mu m^2\ mN^{-1} \quad ,$$
$$S_{MN} = S_{NM} = 0.0113\ \mu m\ mN^{-1} \quad ,$$
$$S_{PM} = S_{MP} = 0.0367\ \mu m\ mN^{-1} \quad .$$

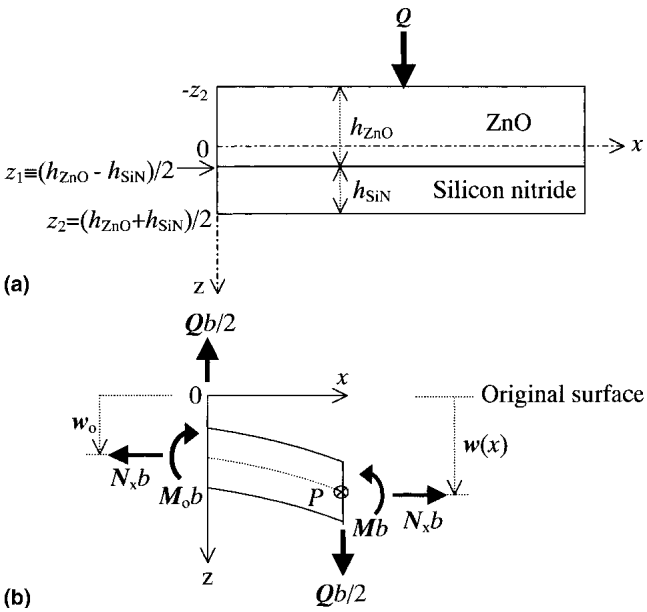

FIG. 2. (a) Cross section of a double-layered ZnO/silicon nitride microbridge. (b) Moments and forces acting on a segment.

Equations (2) and (3) are most convenient to be solved numerically. The method is to assign a set of trial values for E_{SiN} and N^r_{SiN} first. For a particular load Q_i, the numerical solutions of N_{xi} and M_{oi} are attained. The values of Q_i, N_{xi}, and M_{oi} are then plugged into Eq. (1) to calculate the corresponding displacement $w(Q_i, E_{SiN}, N^r_{SiN})$. This process is repeated for many Q_i covering the load range of the experimental measurement. A theoretical curve of w versus Q is thus derived. The deviation between this theoretical curve and the experimental data $w_{exp}(Q_i)$ is quantified by a number defined as:

$$\text{Error} = \sum_i [w_{exp}(Q_i) - w(Q_i, E_{SiN}, N^r_{SiN})]^2 \quad . \tag{8}$$

This value is minimized by trying different trial values of E_{SiN}* and N^r_{SiN}*, and those corresponding to the best fit are used to represent the elastic modulus and residual force per unit width of the silicon nitride film. The internal stress in the film is thus equal to:

$$\sigma^r_{SiN}{}^* = N^r_{SiN}{}^*/h_{SiN} \quad . \tag{9}$$

During bending, the tensile stress at the midpoint of the lower surface of the silicon nitride microbridge should be the largest. The tensile stress recorded just before fracture is believed to be equal to the tensile strength ($\sigma^{TenStren}_{SiN}$) of the silicon nitride film and is easily calculated from the expression:

$$\sigma^{TenStren}_{SiN} = \frac{N_x}{h_{SiN}} - \frac{E_{SiN}h_{SiN}}{2}\left.\frac{d^2w}{dx^2}\right|_{x=l/2} \quad . \tag{10}$$

E_{SiN}*, N^r_{SiN}*, and $\sigma^{TenStren}_{SiN}$ are thus determined and used in the analysis of the double-layered structure as described in the next section.

B. Double-layered ZnO/silicon nitride microbridges

As shown in Fig. 2(a), the x axis is set to coincide with the geometrical central line of a double-layered microbridge along the length. The surfaces of the ZnO layer and silicon nitride layer are at $z = -z_2$, and $z_2 = (h_{ZnO} + h_{SiN})/2$, respectively. The interface between the two layers is at $z_1 \equiv (h_{ZnO} - h_{SiN})/2$. The vertical displacement of the microbridge at $x = l/2$ versus a load per unit width $\boldsymbol{Q}$ is:[9]

$$\boldsymbol{w}(l/2) = -\frac{\boldsymbol{Q}\tanh(\boldsymbol{K}\,l/2)}{2N_x\boldsymbol{K}} + \frac{\boldsymbol{Q}l}{4N_x} - \frac{\overline{\boldsymbol{M}}_o}{N_x}\left[\frac{1}{\cosh(\boldsymbol{K}\,l/2)} - 1\right] + \boldsymbol{S}_{PN}(N_x - N_r) + S_{PP}\frac{\boldsymbol{Q}}{2} - \boldsymbol{S}_{PM}[\boldsymbol{M}_o - \boldsymbol{M}_r] \quad . \tag{11}$$

In the equation, N_x is the total force per unit width acting along the x direction, and M_o is the bending moment per unit width acting on the cross section of the microbridge at $x = 0$ [Fig. 2 (b)]. If the residual stress and elastic modulus of the ZnO layer are denoted to be $\sigma^r{}_{ZnO}$ and E_{ZnO}, respectively, the following quantities are defined:

$$K = \sqrt{\frac{N_x}{B - A^2/D}}$$

$$A = h_{SiN}\, h_{ZnO}\, (E_{SiN}{}^* - E_{ZnO})/2$$

$$B = [E_{SiN}{}^*\, h_{SiN}(h_{SiN}{}^2 + 3\, h_{ZnO}{}^2) + E_{ZnO}\, h_{ZnO}(3\, h_{SiN}{}^2 + h_{ZnO}{}^2)]/12$$

$$D = E_{SiN}{}^*\, h_{SiN} + E_{ZnO}\, h_{ZnO}$$

M_r = residual moment per width = $h_{SiN}\, h_{ZnO}\, (\sigma^r{}_{SiN}{}^* - \sigma^r{}_{ZnO})/2$

N_r = residual force per width = $\sigma^r{}_{SiN}{}^*\, h_{SiN} + \sigma^r{}_{ZnO}\, h_{ZnO}$

$$\overline{M}_o = M_o - (N_x - N_r)A/D - M_r \quad .$$

Two simultaneous equations correlating M_o and N_x are derived. They are:

$$(M_o - M_r)[S_{MM}N_x + K\tanh(K\,l/2)] = S_{MN}N_x(N_x - N_r) + \frac{S_{MP}QN}{2} + \frac{KA(N_x - N_r)}{D}\tanh(K\,l/2) + \frac{Q}{2}\left[\frac{1}{\cosh(K\,l/2)} - 1\right] \quad , \tag{12}$$

$$S_{NN}(N_x - N_r) + \frac{S_{NP}Q}{2} - S_{NM}(M_o - M_r) = \Xi + \frac{A}{D}\left[\frac{Q(\cosh(K\,l/2) - 1)}{2N_x\cosh(K\,l/2)} + \overline{M}_o\frac{K}{N_x}\tanh(K\,l/2)\right] - \frac{l(N_x - N_r)}{2D} \quad , \tag{13}$$

where

$$\Xi = \frac{Q^2}{8KN_x^2}\left[\left(\Lambda^2 + \Psi^2 + \frac{1}{2}\right)K\,l + 4(\Lambda - \Psi)\sinh(K\,l/2) + 2\Lambda\Psi K\,l\cosh(K\,l) + (\Lambda^2 + 2\Lambda\Psi - \Psi^2 + 4\Psi)\sinh(K\,l) + \Psi^2\sinh(2K\,l)\right] \quad ,$$

$$\Lambda = -\frac{\sinh(K\,l/2)}{\sinh(K\,l)} - \frac{\overline{M}_o K}{Q\sinh(K\,l)} \quad ,$$

$$\Psi = \frac{\overline{M}_o K}{Q\sinh(K\,l)} \quad .$$

S_{ij} (i, j = P, M, N) are the compliances of the silicon substrate. The appearance of the terms containing S_{ij} in Eqs. (11)–(13) is due to the deformability of the substrate, and according to finite element analysis (Su):[9]

$$S_{NN} = 0.0349\ \mu m^2\ mN^{-1} \quad ,$$

$$S_{PP} = 0.106\ \mu m^2\ mN^{-1} \quad ,$$

$$S_{MM} = 0.0351\ mN^{-1} \quad ,$$

$$S_{NP} = S_{PN} = 0.0361\ \mu m^2\ mN^{-1} \quad ,$$

$$S_{MN} = S_{NM} = 0.00495\ \mu m\ mN^{-1} \quad ,$$

$$S_{PM} = S_{MP} = 0.0211\ \mu m\ mN^{-1} \quad .$$

Equations (12) and (13) are solved numerically by setting E_{ZnO} and $\sigma^r{}_{ZnO}$ to be equal to some trial values. At a particular load Q_i, they are solved to get some numerical values of M_{oi} and N_{xi}. Then, Q_i, M_{oi}, and N_{xi} are plugged into Eq. (11) to calculate the corresponding displacement $w(Q_i, E_{ZnO}, \sigma^r{}_{ZnO})$. A theoretical curve of w versus Q is derived. The deviation between the theoretical curve and the experimental data is represented by a number:

$$\textbf{Error} = \sum_i [w_{exp}(Q_i) - w(Q_i, E_{ZnO}, \sigma^r{}_{ZnO})]^2 \quad . \tag{14}$$

This number is then minimized by trying different trial values of E_{ZnO} and $\sigma^r{}_{ZnO}$. The settings corresponding to the best fit are denoted as $E_{ZnO}{}^*$ and $\sigma^r{}_{ZnO}{}^*$ and are used to represent the elastic modulus and internal stress of the ZnO layer.

The internal stresses at a certain point (x, z) in the ZnO layer and a certain point (x, z) in the silicon nitride layer can be expressed as:

$$\sigma_{ZnO}(x, z) = E_{ZnO}{}^*\left[\left(\frac{A}{D} - z\right)\frac{\partial^2 w}{\partial x^2} + \frac{N_x - N_r}{D}\right] + \sigma^r{}_{ZnO}{}^* \quad (z = -z_2 \text{ and } z_1) \quad , \tag{15}$$

$$\sigma_{SiN}(x, z) = E_{SiN}{}^*\left[\left(\frac{A}{D} - z\right)\frac{\partial^2 w}{\partial x^2} + \frac{N_x - N_r}{D}\right] + \sigma^r{}_{SiN}{}^* \quad (z = -z_2 \text{ and } z_1) \quad . \tag{16}$$

In the current case, the tensile stress within the silicon nitride layer would never exceed the measured $\sigma^{TenStren}{}_{SiN}$ (to be illustrated in Sec. IV. B). One can therefore assert that for a double-layered microbridge under increasing load, somewhere on the top surface of the ZnO layer cracks first (normally at one of the two ends), and at that load the silicon nitride layer has not yet broken.

IV. RESULTS AND DISCUSSION

A. Single-layered silicon nitride microbridges

We present the results on the silicon nitride microbridges in this section. Figure 3(a) shows the typical load–displacement curve for a single-layered silicon nitride microbridge. With increasing load, the displacement increases and eventually the microbridge breaks (labeled as the fracture point in the figure). The occurrence of fracture is identified by a sudden drop in load, accompanied by a drastic rise in displacement (not shown). The dashed line as shown in Fig. 3(a) is the theoretical best fit to the experimental data. The exaggeration of the fitting at low load range is shown in Fig. 3(b), indicating that the fitting is quite satisfactory. The fitting to each curve gives estimates of E_{SiN}* and σ^{r}_{SiN}*. The data of E_{SiN}* corresponding to the specimens of different widths are shown in Fig. 4. The average of the data points is denoted as $\langle E_{SiN}^{*} \rangle = 260 \pm 20$ GPa (Table I), and is used to represent the elastic modulus of the silicon nitride film. The standard deviation of the data points gives the estimate of the error of this quantity.

We notice that the value of $\langle E_{SiN}^{*} \rangle$ is very close to 249 GPa of the bulk stoichiometric Si_3N_4.[12] On the other hand, the elastic modulus of the silicon nitride film was measured by conventional nanoindentation test with the presence of the substrate. The nanoindentation elastic modulus determined with this technique (E_{SiN}^{indent}) is

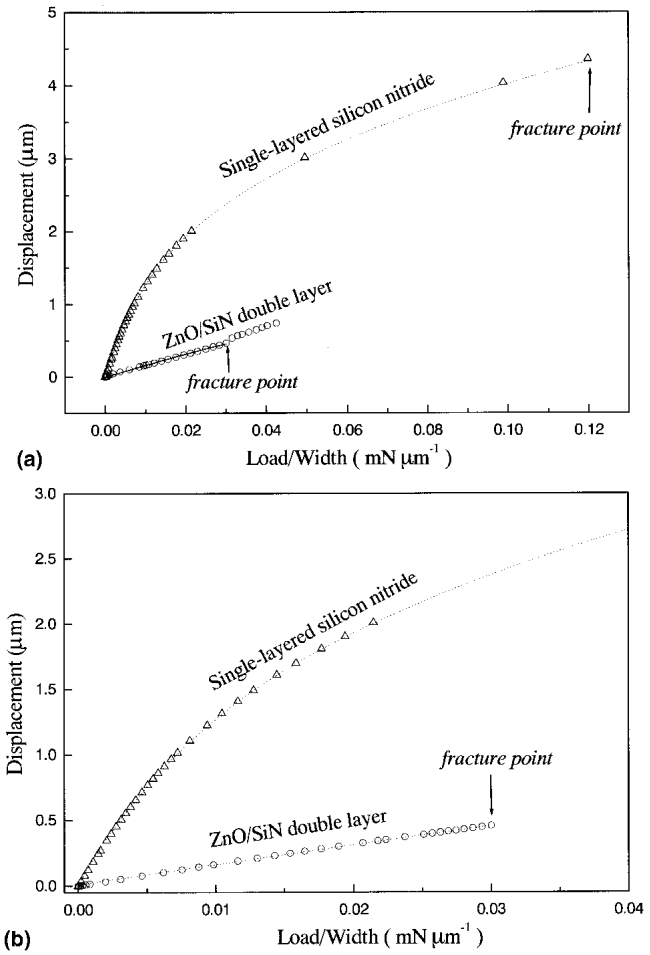

FIG. 3. Typical load–displacement curve of (a) single-layered silicon nitride microbridge (Δ) and a double-layered ZnO/silicon nitride microbridge (O). Theoretical fittings to the data are shown. (b) Magnified features in the low-load range.

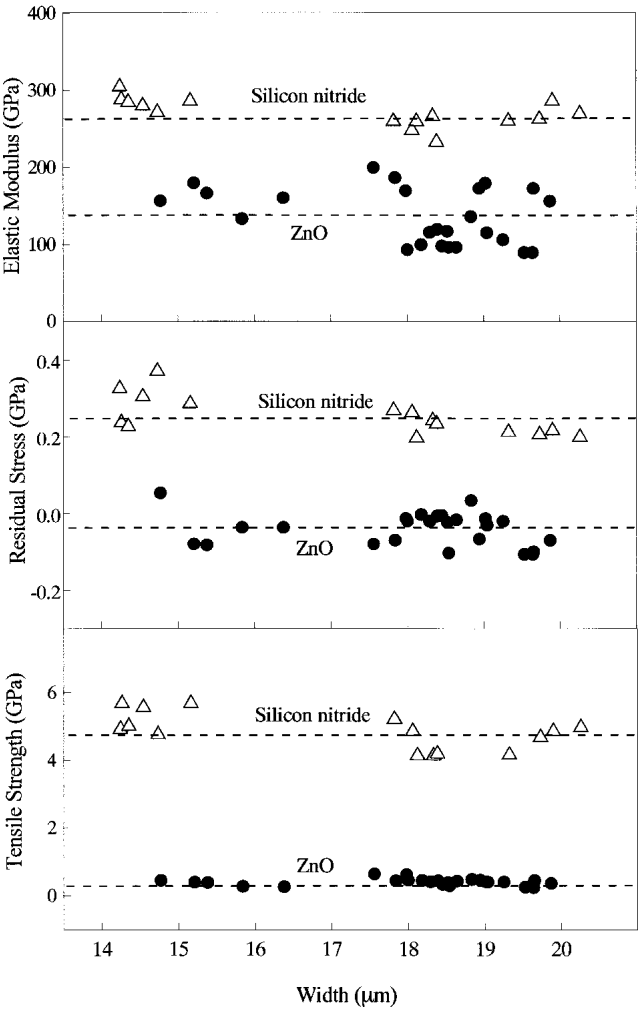

FIG. 4. Mechanical properties of the silicon nitride and ZnO films determined by microbridge tests. The dashed lines represent the averages of all the data points.

TABLE I. Mechanical properties of silicon nitride and ZnO films obtained by microbridge tests and nanoindentation tests.

Silicon nitride film	ZnO film
$\langle E_{SiN}^{*} \rangle = 260 \pm 20$ GPa	$\langle E_{ZnO}^{*} \rangle = 137 \pm 18$ GPa
$\langle E_{SiN}^{indent} \rangle = 251 \pm 14$ GPa	$\langle E_{ZnO}^{indent} \rangle = 143 \pm 14$ GPa
$\langle \sigma^{r}_{SiN}{}^{*} \rangle = 0.25 \pm 0.028$ GPa	$\langle \sigma^{r}_{ZnO}{}^{*} \rangle = -0.041 + 0.02$ GPa
$\langle \sigma^{TenStren}_{SiN} \rangle = 4.8 \pm 0.7$ GPa	$\langle \sigma^{TenStren}_{ZnO} \rangle = 0.412 \pm 0.05$ GPa

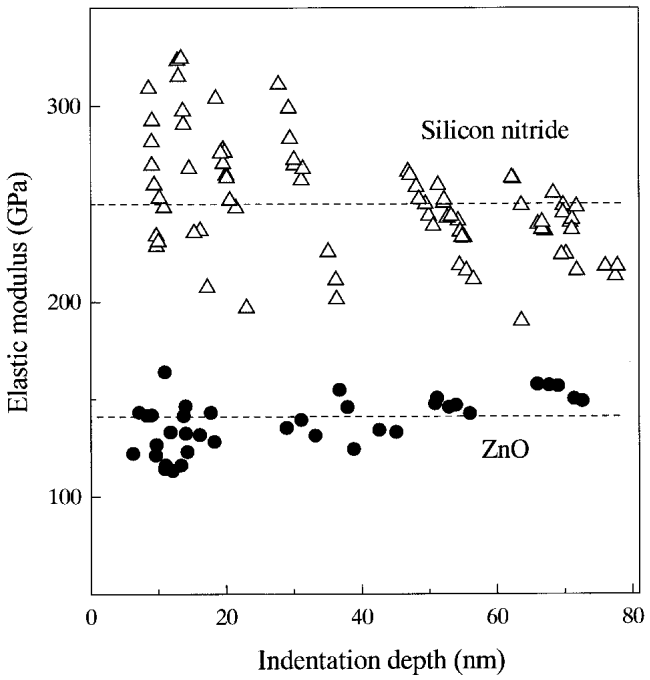

FIG. 5. Elastic modulus of the silicon nitride and ZnO films measured by nanoindentation tests.

plotted as a function of contact depth h_c in Fig. 5. The data points corresponding to contact depths in the range of 7.6 nm $\leqslant h_c \leqslant$ 226 nm are averaged to give a representative result $\langle E_{SiN}{}^{indent} \rangle = 251 \pm 14$ GPa. This result is rather close to $\langle E_{SiN}{}^{*} \rangle$, further supporting the validity of the microbridge method.

$\sigma^{r}{}_{SiN}{}^{*}$ of the samples with different widths are also plotted in Fig. 4. The sign of all the $\sigma^{r}{}_{SiN}{}^{*}$ values is positive, indicating that the as-deposited silicon nitride film is under tensile stress. The data are averaged to give a number $\langle \sigma^{r}{}_{SiN}{}^{*} \rangle = 0.25 \pm 0.028$ GPa (Table I), which is the best estimate of the tensile stress of the silicon nitride film. The standard deviation gives the error of the measurements. The internal stress of silicon nitride films is found to depend strongly on the methods of deposition. In a recent study, we proposed that the condition of particle bombardment on the growing surface was critical in affecting the internal stress of silicon nitride films.[13] For silicon nitride films prepared by LPCVD process involving species with thermal energies as low as ≈0.1 eV, the internal stress is tensile and falls in the range of 0.29 to 1 GPa.[10,14] The value of $\langle \sigma^{r}{}_{SiN}{}^{*} \rangle$ of our silicon nitride films is basically consistent with the range generally observed for LPCVD silicon nitride films (though just slightly below).

Figure 4 also shows the data points of the tensile strength $\sigma^{TenStren}{}_{SiN}$ of the silicon nitride film obtained from the microbridges of different widths [Eq. (10)]. The data are averaged to give the best estimate of the tensile strength of the silicon nitride film, which is equal to $\langle \sigma^{TenStren}{}_{SiN} \rangle = 4.8 \pm 0.7$ GPa. Cardinale *et al.*[7] proposed a fracture strength of 0.39 GPa for silicon-rich plasma-assisted dry soldering a silicon nitride films and 0.42 GPa for the nitrogen-rich silicon nitride films based on bulge tests. Budinski *et al.*[15] quoted a result of 0.800 GPa for the flexural strength of bulk silicon nitride. Yang *et al.*[16] proposed a higher tensile strength of 10.8 to 11.7 GPa for LPCVD silicon nitride films measured by bulge tests. Zhang *et al.*[10] reported an even higher level of 12.26 GPa for LPCVD silicon nitride films by microbridge tests. Our result of $\langle \sigma^{TenStren}{}_{SiN} \rangle$ falls in the range formed by these data. We further notice that an *ab initio* theory predicts that the tensile strength of the ideal beta-silicon nitride lattice can be as high as 72.2 and 75 GPa for hypothetical uniaxial tensile loads applying along the [100] and [001] directions, respectively.[17] These spectacular predicted values are not observed experimentally because in real situations, the surface of a ceramic material generally contains flaws. Under the influence of tension, stress concentration occurs at the tips of the flaws, so that the experimentally observed tensile strength of a ceramic material is always lower than that expected for the ideal defect-free structure.

B. Double-layered ZnO/silicon nitride microbridges

With the above results for the silicon nitride, analysis on double-layered microbridges was carried out. The results are presented as follows. Figure 3(a) shows the typical load–displacement curve of a double-layered ZnO/silicon nitride microbridge of a width equal to 18 μm. The fitting of the analytic solution to the experimental data is shown by the solid line. Exaggeration of the fitting to the data at low load range is shown in Fig. 3(b). Importantly, a kink is seen in the load–displacement curve. The kink is supposed to be due to the fracture of the ZnO layer. One may imagine that the cracking of the ZnO layer gives rise to an abrupt discontinuity of the slope of the load–displacement curve. For all the tests on the double-layered specimens, the load for this initial cracking kink did not exceed the tensile strength of the silicon nitride film $\langle \sigma^{TenStren}{}_{SiN} \rangle$, and so at this load the silicon nitride layer has not broken.

The fitting to each load–displacement curve gives an estimate to the elastic modulus ($E_{ZnO}{}^{*}$) of the ZnO layer. The data of the microbridges with different widths are plotted in Fig. 4, which are averaged to give the best estimate of the elastic modulus $\langle E_{ZnO}{}^{*} \rangle = 137 \pm 18$ GPa. Figure 5 shows the nanoindentation elastic modulus as a function of h_c. The average of the data point in the range of 22 nm < h_c < 90 nm is $\langle E_{ZnO}{}^{indent} \rangle = 143 \pm 14$ GPa, which is found to be fairly close to $\langle E_{ZnO}{}^{*} \rangle$. In addition, $\langle E_{ZnO}{}^{indent} \rangle$ is also consistent with those reported by

many groups. Jade *et al.*[18] reported a range of 146.2 to 241.5 GPa for ZnO films by using resonance method. Kucheyev *et al.*[19] recently reported a different result. They carried out nanoindentation tests on bulk ZnO single-crystal with the load applying along the *c* axis of the hexagonal structure. The detected elastic modulus was 111.2 GPa and was smaller than our current result. The deviation may be explained by the occurrence of plastic slip between lattice planes along the *c* axis in the experiment of Kucheyev and colleagues.

The data $\sigma^{r}{}_{ZnO}{}^{*}$ obtained from the fitting to the data of the microbridges of different widths are shown in Fig. 4. They are averaged to give the best evaluation of the residual stress of the ZnO film (i.e., $\langle\sigma^{r}{}_{ZnO}{}^{*}\rangle = -0.041 \pm 0.02$ GPa). The minus sign indicates that the ZnO layer experiences a compressive stress. Referring to published results from different groups, it is found that the internal stress of ZnO films depends sensitively on the fabrication conditions. Gupta *et al.*[20] reported that ZnO film prepared by sputtering at low temperature had a compressive stress of –1.66 GPa. Indeed, at a low substrate temperature the atoms were less mobile, so that the compressive stress established by the peening effect was basically not released.[21] With increasing substrate temperature, the internal stress changed from compressive to tensile, because crystallization occurred, and the atoms were more ready to rearrange so to release the internal stresses.[20] Similar interpretation was applied to explain the ambient pressure dependence of the internal stresses in ZnO films prepared by sputtering. At low ambient pressure, the sputtered species reached the substrate with higher kinetic energy and caused more severe peening effect, so that greater compressive stress was built up in the deposits.[21] On the contrary, at high ambient pressure, the sputtered species collided more frequently and gained random thermal motion in the way of approaching the substrate. As a consequence, the peening effect was less severe, and the deposits were less compressively stressed. Hinze *et al.*[22] found that ZnO films deposited at a lower ambient pressure of 0.5 mtorr by magnetron sputtering had a high compressive stress of ≈ –1.5 GPa. By increasing the ambient pressure, the internal stresses changed from being compressive to tensile. Zero stress was found to occur at an intermediate pressure of 2 mtorr. In our case, we used moderate substrate temperature (400 °C) and pressure (7 mtorr), so that the ZnO films were found to have a low stress level of $\langle\sigma^{r}{}_{ZnO}{}^{*}\rangle = -0.041 \pm 0.02$ GPa.

Next, we analyze the stress distribution in the double-layered structure at the load of the kink in Fig. 3(a) (initial fracture point). At the surface of the ZnO layer ($z = -z_2$), the stress as a function of x from 0 to $l/2$ is calculated from Eq. (15). Results are shown in Fig. 6. In particular, the stress at $x = 0$ is tensile. Its magnitude decreases with increasing x and eventually becomes

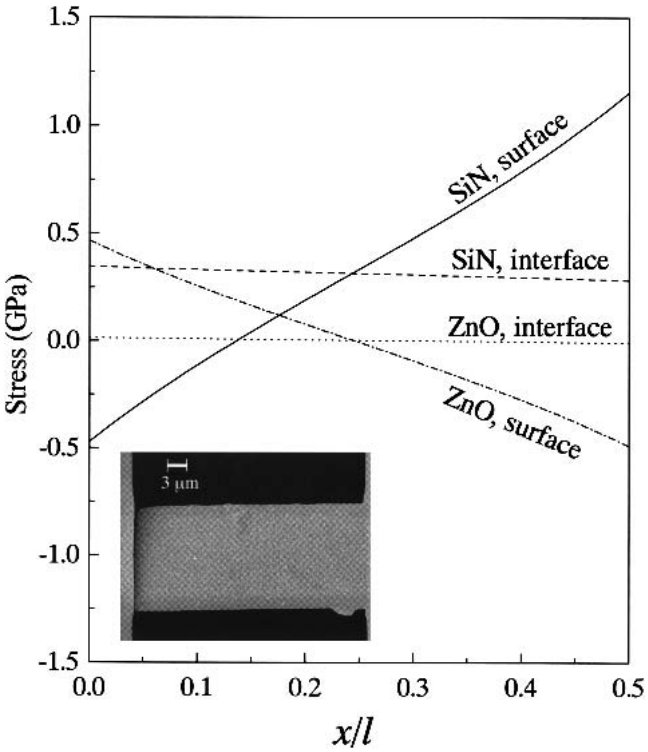

FIG. 6. Stresses on the ZnO surface; on the silicon nitride surface; and at their interface evaluated at the load of the initial fracture point. The inset shows a SEM image of a broken double-layered microbridge.

compressive. Similarly, the stress at the surface of the silicon nitride layer ($z = z_2$) with x varying from 0 to $l/2$ was determined from Eq. (16). At $x = 0$, the stress is compressive. Its magnitude drops with increasing x and eventually becomes tensile. The stresses besides the interface of the two layers ($z = z_1$) are also calculated from the two equations and plotted in Fig. 6. We notice that at the initial fracture point, the maximum tensile stress experienced by the silicon nitride layer ($x/l = 0.5$) does not exceed its tensile strength $\langle\sigma^{TenStren}{}_{SiN}\rangle$, so that the silicon nitride layer does not fracture. In other words, the appearance of the kink is due to the fracture of the ZnO layer, and the fracture point should be at $x = 0$ where the tensile stress is the largest. The validity of this reasoning is verified by the SEM image as shown in the inset of Fig. 6, where a crack is found to appear at the junction between the microbridge and the substrate.

Based on the above discussion, the tensile strength of the ZnO layer is assumed to be equal to the tensile stress ($\sigma^{TenStren}{}_{ZnO}$) in the ZnO layer at $x = 0$ at the load of the kink. The data points of $\sigma^{TenStren}{}_{ZnO}$ of the microbridges of different widths are obtained and plotted in Fig. 4. In Fig. 7, $\sigma^{TenStren}{}_{ZnO}$ of the microbridges of different lengths are plotted. (Also shown in Fig. 7 are the calculated tensile stress experienced by the silicon nitride layer at the midpoint of its surface at the load when the ZnO layer cracks. It is always lower than $\langle\sigma^{TenStren}{}_{SiN}\rangle$,

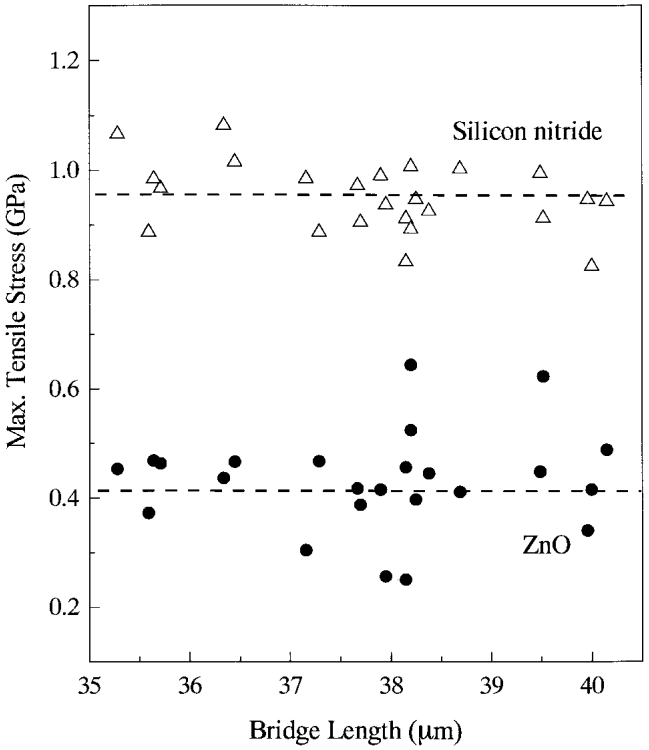

FIG. 7. Stresses on the ZnO surface at $x = 0$ (Δ) and on the silicon nitride surface at $x = l/2$ (●) evaluated at the load of the fracture point of the ZnO layer.

indicating that silicon nitride layer has not broken when the ZnO undergoes its initial crack.) The data points of $\sigma^{\text{TenStren}}{}_{\text{ZnO}}$ are averaged to give the best estimate of the tensile strength of the ZnO layer (i.e., $\langle\sigma^{\text{TenStren}}{}_{\text{ZnO}}\rangle = 0.412 \pm 0.05$ GPa) (Table I). To our knowledge, the tensile strength of ZnO thin film is seldom reported in the literature. We therefore refer to the results reported by Lu *et al.*[23] for bulk ZnO ceramics for comparison. They claimed that the mechanical strength of bulk ZnO ceramics lied in the range of 0.102 to 0.105 GPa, which was roughly 25% of $\langle\sigma^{\text{TenStren}}{}_{\text{ZnO}}\rangle$ as observed in this study.

The results indicate that the tensile strength of ZnO film is relatively low; namely, just 0.08 times that of silicon nitride. Comparison made with silicon nitride means that silicon nitride is a widely used structural ceramic material and serves fairly well as a reference. We therefore asserted that if a ZnO film is used in a device, the risk of fracture must be taken into careful consideration.

V. CONCLUSIONS

Single-layered silicon nitride and double-layered ZnO/silicon microbridges were fabricated. The former was fabricated by the LPCVD method followed by photolithography/dry etching process. The latter was formed by sputtering ZnO films on the single-layered silicon nitride microbridges. Microbridge tests were carried out to determine the elastic modulus, internal stress, and tensile strength of the two film materials.

For the silicon nitride films, the elastic modulus, internal stresses, and tensile strength were determined to be 260 ± 20, 0.25 ± 0.028, and 4.8 ± 0.7 GPa, respectively. The result of the elastic modulus obtained by this method is in good agreement with that attained by using nanoindentation tests. Most of the single-layered microbridges were found to fracture at the midpoint. The corresponding tensile stress experienced by this part of the microbridge just before fracture is assigned to be the tensile strength of the silicon nitride film.

The elastic modulus, internal stresses, and tensile strength of the ZnO films were determined to be 137 ± 18 GPa, −0.041 ± 0.02 GPa (compressive), and 0.412 ± 0.05 GPa, respectively. The result of the elastic modulus determined by this method is consistent with that obtained by nanoindentation tests (143 ± 14 GPa). Cracking was found to initiate on the top surface of the ZnO layer at one end of the microbridge. The tensile stress at this position just before cracking is assumed to be the tensile strength of the ZnO layer $\langle\sigma^{\text{TenStren}}{}_{\text{ZnO}}\rangle$. Most importantly, the value of $\langle\sigma^{\text{TenStren}}{}_{\text{ZnO}}\rangle$ provides a useful guideline, where a ZnO film used in a device must be prevented from experiencing a tensile stress exceeding this level.

ACKNOWLEDGMENTS

This work was supported by the Center for Smart Materials (Code: 1.A.310), an internal grant from the Hong Kong Polytechnic University (Code: G-T 594), and by the Hong Kong Innovation and Technology Fund (ITF) (Code: K.11.2A.ZP07). The work was also supported by Chinese National Project, No. 1999033103. We are also indebted to the efforts from Miss M.P. Tsang in doing some preliminary work on the micromachining of microbridges.

REFERENCES

1. C-H. Dan and E.S. Kim, in *Proceedings of the Fourteenth IEEE International Conference on Micro Electro Mechanical Systems* (2001), p. 110.
2. Y-J. Yong, Y-S.Kang, P.S. Lee, and J-Y. Lee, J. Vac. Sci. Technol. B **20,** 42 (2002).
3. S.H. Park, B.C. Seo, G. Yoon, and H.D. Park, J. Vac. Sci. Technol. A **18,** 2432 (2000).
4. Committee on Advanced Materials and Fabrication Methods for Microelectromechanical Systems, *Microelectromechanical Systems: Advanced Materials and Fabrication Methods* (National Academy Press, Washington D.C., 1997), p. 2.
5. X. Gong and Z. Suo, J. Mech. Phys. Solids **44,** 751 (1996).
6. S.L. dos Santos e Lucato, H-A. Bahr, V-B. Pham, D.C. Lupascu, H. Balke, J. Rödel, and U. Bahr, J. Mech. Phys. Solids **44,** 751 (2002).

7. G.F. Cardinale and R.W. Tustison, Thin Solid Films **207,** 126 (1992).
8. J.J. Vlassak and W.D. Nix, J. Mater. Res. **7,** 3242 (1992).
9. Y-J. Su, C-F. Qian, M-H. Zhao, and T-Y. Zhang, Acta Mater. **48,** 4901 (2000).
10. T-Y. Zhang, Y-J. Su, C-F. Qian, M-H. Zhao, and L-Q. Chen, Acta Mater. **48,** 2843 (2000).
11. W.C. Oliver and G.M. Pharr, J. Mater. Res. **7,** 1564 (1992).
12. D.M. Teter, MRS Bull. **23,** 22 (1998).
13. M.P. Tsang, C.W. Ong, N. Chong, C.L. Choy, P.K. Lim, and W.W. Hung, J. Vac. Sci. Technol. A **19,** 2542 (2001).
14. A.C. Adam, in *VLSI Technology*, edited by S.M. Sze (McGraw-Hill, Singapore, 1985), p. 120.
15. K.G. Budinski and M.K. Budinski, *Engineering Materials: Properties and Selection*, 6th ed. (Prentice Hall, Englewood Cliffs, NJ, 1999), p. 694.
16. J.L. Yang and O. Paul, Sens. Actuators A **97–98,** 520 (2002).
17. S. Ogata, N.Hirosaki, C. Kocer, and H. Kitagawa, Phys. Rev. B **64,** article 172102 (2001).
18. S.A. Jade and J.G. Smith, IEEE Trans. Ultrason., Ferroelect., Freq. Contr. **46,** 768 (1999).
19. S.O. Kucheyev, J.E. Bradby, J.S. Williams, C. Jagadish, and M.V. Swain, Appl. Phys. Lett. **6,** 956 (2002).
20. V. Gupta and A. Mansingh, J. Appl. Phys. **80,** 1063 (1996).
21. A. Cimpoiasu, N.M. van der Pers, Th.H. de Keyser, A. Venema, and M.J. Vellekoop, Smart Mater. Struct. **5,** 744 (1996).
22. J. Hinze and K. Ellmer, J. Appl. Phys. **88,** 2443 (2002).
23. C. Lu, R. Danzer, and F.D. Fischer, Phys. Rev. E **65,** article 067102 (2002).